Journal of Cleaner Production 223 (2019) 238–251

Contents lists available at ScienceDirect

Journal of Cleaner Production

journal homepage: www.elsevier.com/locate/jclepro

Exploring the trend, prediction and driving forces of aerosols using satellite and ground data, and implications for climate change mitigation

Xueke Li [a, *], Chuanrong Zhang [a], Weidong Li [a], Richard O. Anyah [b], Jing Tian [c]

[a] Department of Geography, University of Connecticut, Storrs, CT 06269, USA
[b] Department of Natural Resources and the Environment, University of Connecticut, Storrs, CT 06269, USA
[c] Key Laboratory of Water Cycle & Related Land Surface Processes, Institute of Geographic Sciences and Natural Resources, Chinese Academy of Sciences, Beijing 100101, China

ARTICLE INFO

Article history:
Received 29 March 2018
Received in revised form
27 December 2018
Accepted 11 March 2019
Available online 14 March 2019

Keywords:
MODIS C6
Aerosol optical depth
Time series
ARIMA
Climate change mitigation

ABSTRACT

Human activities-related aerosol emissions and CO_2 emissions originate from many of the common sources. Identifying the aerosol variations and the underling determinates can provide insights into united mitigation policy controls targeting on both aerosol pollution and climate change. Long-term trend analysis and modeling offers an effective way to fully appreciate how aerosols interlink with carbon cycle and climate change. This study analyzes the current trends, models the future predictions, and investigates potential driving forces of aerosol loading at six sites across North America and East Asia during 2003–2015. Satellite-retrieved MODIS Collection 6 retrievals and ground measurements derived from AERONET are used. Results show that there is a persistent decreasing trend in AOD for both MODIS data and AERONET data at three sites. Monthly and seasonal AOD variations reveal consistent aerosol patterns at sites along mid-latitudes. Regional differences caused by impacts of climatology and land cover types are observed for the selected sites. Statistical validation of time series ARIMA models indicates that the non-seasonal ARIMA model performs better for AERONET AOD data than for MODIS AOD data at most sites, suggesting the method works better for data with higher quality. The seasonal ARIMA model reproduces time series with distinct seasonal variations much more precisely. The reasonably predicted AOD values could provide reliable estimates to better inform the decision-making for sustainable environmental management. Drawn from aerosol pollution control strategies, it is suggested that the enforcement of regulations on emission sources and the initiative of reforestation on emission sinks could have potential implications for climate change mitigation.

1. Introduction

In the context of rapid industrialization and urbanization, climate change and air quality impose two major threats on sustainability. Notorious and historical examples range from the Los Angeles Photochemical Smog first identified in 1942, the historic London fog in 1952, to the recent/current heavily polluted megacities such as Beijing and Delhi (Shi et al., 2016; Wang et al., 2016). Aerosols, being one of the major culprits for air pollution, are demonstrated to have great adverse impacts on human health (Brunekreef and Holgate, 2002). Aerosols that originated from common anthropogenic sources responsible for greenhouse gas (GHG) emissions such as biomass burning and fossil fuel combustion strongly interlink with carbon cycle (Andreae and Merlet, 2001; Meng et al., 2016) and climate change (Casazza et al., 2018; Ramanathan and Carmichael, 2008). This interconnectedness provides insights into united mitigation policy controls targeting on both aerosol pollution and climate change, which may counteract a considerable portion of mitigation costs (IPCC, 2013).

Identifying the current trend, the future predictions, and the underlying driving forces of aerosol properties facilitates identification of appropriate air pollution mitigation policies targeting on common sources and sinks relevant to carbon reduction. In view of this, various measurement methods have been employed in this study to observe, analyze and characterize aerosol properties,

* Corresponding author.
E-mail address: xueke.li@uconn.edu (X. Li).

https://doi.org/10.1016/j.jclepro.2019.03.121
0959-6526/

ranging from ground-based monitoring networks to data retrievals from satellite imagery. For example, the AErosol RObotic NETwork (AERONET) (Holben et al., 1998) – one of the primary ground monitoring systems, provides worldwide measurements of aerosol properties, such as aerosol optical depth (AOD), a measure of total column light extinction, and Ångström exponent (AE), a parameter inversely correlated with aerosol particle size (Dubovik et al., 2000). Despite the high precision of the *in situ* measurements, their spatial coverage is limited (Li et al., 2017). As a complementary data source, satellite remotely sensed imagery offers spatiotemporally continuous products. Among various satellite-retrieved AOD products, MODerate resolution Imaging Spectroradiometer (MODIS) retrieval data has been demonstrated to be a quality-assured dataset and the recently released Collection 6 (C6) has significant improvement over the previous collections (Levy et al., 2013).

In recent years, extensive efforts have been made to assess the long-term trends of aerosol loading. Zhang and Reid (2010) reported regional differences in AOD trends using MODIS and Multi-angle Imaging Spectroradiometer (MISR) products. Hsu et al. (2012) found a weakly increasing tendency over ocean in AOD retrieved from Sea-viewing Wide Field-of-view Sensor (SeaWiFS). Other studies observed upward trends of AOD over economically growing/industrialized regions of Asia and downward trends of AOD over the eastern United States (US) and Europe using data either from ground measurements (Li et al., 2014) or satellite sensors (Zhang et al., 2016). Although trend analysis of aerosols has been well documented in previous studies, statistical future prediction of aerosol patterns and the underlying causes that explain these changes in aerosol concentrations remain less well known. Time series analysis (TSA) provides a suite of methodologies and techniques to extract useful information and reduce noise by simulating, estimating, and forecasting future trends from reliable identification of past temporal modes in variables. Within this domain, autoregressive integrated moving average (ARIMA) models introduced by Box and Jenkins (1970) have been successfully applied in the fields of economics (French et al., 1987; Granger and Newbold, 2014), agriculture (Jiang et al., 2010; Xiao et al., 2011), forestry (Huesca et al., 2014), and hydrology (Gemitzi and Stefanopoulos, 2011). A recent study by Soni et al. (2016) explored the possibility of ARIMA model to serve as an indicator to evaluate the accuracy of satellite AOD data in comparison with ground AOD data. Nevertheless, it is uncertain whether the performance of the model or the retrieved aerosol profile could be influenced by the microphysical, climatological and some extrinsic properties of aerosols.

This article presents a comprehensive study of aerosols over six featured sites spreading across North America (NA) and East Asia using data from MODIS C6 and AERONET during 2003–2015. These sites are of particular interest because they are characterized by similar/dissimilar geographic features, climatological conditions, land cover and fuel types (Tie et al., 2006). We analyze the trend and main contributors of aerosol variations, and explore the applicability of using the ARIMA method to model recent AOD time series data and forecast future AOD values. Meanwhile, potential determinants that may lead to uncertainties in the model is also assessed. The main questions addressed in this study include the following: (1) How did aerosol change during the studied period at annual, seasonal, and monthly timescales and what are the contributors leading to the change? Are there any consistencies or differences in the trend patterns among the six sites? (2) Can the ARIMA model properly predict AOD time series and what is the ideal condition for accurate prediction? And (3) finally, how do factors such as retrieval algorithms, geographic location, land cover, climatology, and missing data affect the prediction performance of the ARIMA model? It is expected that analysis of the case studies could provide some recommendations for reducing aerosol pollution and carbon emissions from both sources and sinks perspectives.

The rest of this paper is structured as follows: Section 2 describes the data sources and methodology used in the study. Section 3 provides an interpretation of the results. Section 4 focuses on the discussion of the results. Section 5 summarizes our major findings.

2. Data and methodology

2.1. Data and site description

The MODIS C6 monthly AOD product (MYD08_M3) obtained from the NASA Goddard Space Flight Center archived database (https://ladsweb.nascom.nasa.gov/data/search.html) was used in this study. This Level 3 Scientific Data Set (SDS) was computed by averaging the Level 2 aerosol product to a $1^\circ \times 1^\circ$ grid. Among many parameters, the combined Dark Target (DT) and Deep Blue (DB) retrievals at 550 nm were selected. Validation of MODIS C6 AOD using the DT algorithm and the DB algorithm has been performed by Levy et al. (2013) and Sayer et al. (2014), separately. The time span of the monthly mean AOD data used in this study is mainly from January 2003 to December 2015.

For evaluating the MODIS AOD product, ground AOD measurements collected from AERONET were also used. Without cloud contamination, AERONET AOD data was reported to have accuracy higher than ±0.01 and ±0.02 for longer (>440 nm) and shorter (<440 nm) wavelengths, respectively (Holben et al., 1998). Thus, it is usually considered as referenced data with high quality in the previous studies (Huang et al., 2016; Xiao et al., 2016). In this study, AERONET Version 2 Level 2.0 monthly AOD averaged data (derived from the daily averaged data) was primarily used. We calculated AOD values at 550 nm wavelength, which were not provided in the ground networks, using the equation followed by previous studies (Bibi et al., 2015; Boiyo et al., 2017) as shown below:

$$AOD_\lambda = AOD_{\lambda_0}\left(\frac{\lambda}{\lambda_0}\right)^{-\alpha} \quad (1)$$

where AOD_λ and AOD_{λ_0} are the AOD values at λ and λ_0 wavelengths, with λ and λ_0 being equal to 550 nm and 440 nm respectively in our study; α is the Ångström coefficient at 440–870 nm. Hereafter, unless specified otherwise, references to AOD indicate AOD at 550 nm.

To ensure a continuous time series of aerosols, ground sites with complete data records in a period of 13 years, and no less than eight months in each year, were primarily considered. As a result, four AERONET sites were chosen. They are GSFC (Goddard Space Flight Center) site, MDSC (MD_Science_Center) site, Boulder (BSRN_BAO_Boulder) site, and the Beijing site. For a comparative study with Beijing site, the Xianghe site (spans from Sep. 2004 to Aug. 2015), which is close to Beijing, was also taken into account. In addition, the CKU (Chen-Kung_Univ) site was selected to account for a thorough analysis of the model's applicability in regions with relatively lower latitude. The geographical distribution of the six selected sites is shown in Fig. 1 and a detailed description of these sites is summarized in Table 1.

Among the six sites, GSFC and MDSC are located in eastern U.S. The region has relatively flat terrain and the major types of land use and land cover are urban and built-up (Liu et al., 2004). Climate in these two sites has the characteristics of the humid subtropical climate. By contrast, Boulder site lies at the foothill of the Rocky Mountains in western U.S. with a high altitude. It is characterized

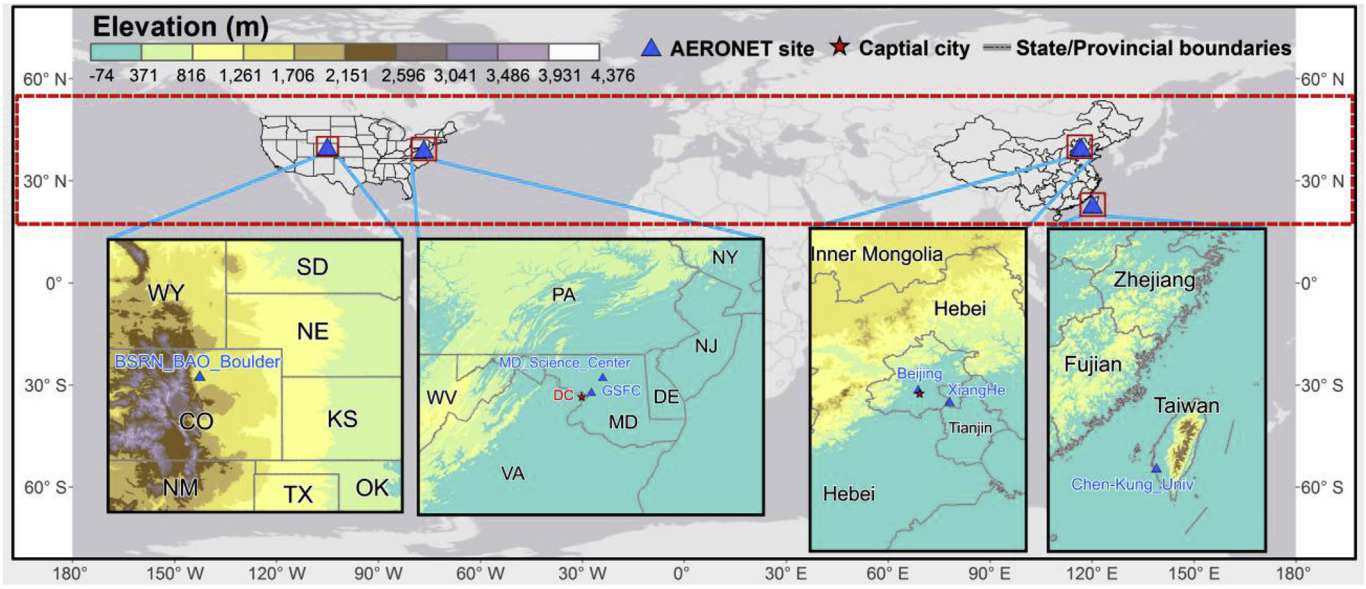

Fig. 1. Geographic locations of the six selected AERONET sites.

Table 1
Description of the six AERONET measurement sites selected for the study.

Site name	Location	Elevation (m)	Dominant Aerosol Type	Literature
GSFC	38.99° N, 76.84° W	87	Urban-Industrial	García et al. (2012)
MDSC (MD_Science_Center)	39.28° N, 76.62° W	15	Urban-Industrial	Kahn et al. (2010)
Boulder (BSRN_BAO_Boulder)	40.05° N, 105.01° W	1604	Continental	Kahn et al. (2010)
Beijing	39.98° N, 116.38° E	92	Mixed	Ichoku et al. (2005)
Xianghe	39.75° N, 116.96° E	36	Mixed	Giles et al. (2012)
CKU (Chen-Kung_Univ)	23.00° N, 120.22° E	50	Mixed	Ocko and Ginoux (2017)

by semi-arid climate and snowfall starts from October to the next April.

Beijing and Xianghe sites are situated in north China, which has a monsoon-influenced humid continental climate. Specifically, Beijing site is located in an urban area of Beijing with the southwest and east areas being highly industrialized (Garland et al., 2009). However, Xianghe site is located in a suburban area of Hebei Province. It is about 70 km southeast of Beijing and is surrounded by agricultural land with few industries. CKU site is located in southern Taiwan. It is within the East Asian monsoon regime (Chou et al., 2006). The area is polluted year-round owing to heavy industries nearby, with seasonal influence of biomass burning and intense dust storm (Chen et al., 2009). Hence, it is categorized as a mixed aerosol type.

Sites of GSFC, MDSC, Boulder, Beijing and Xianghe have varied aerosol feature types, although they lie mainly along the approximate latitude in the northern hemisphere. The sites of GSFC and MDSC are dominated by urban-industrial aerosol type, which is primarily caused by urban-industrial emissions. In addition to impacts from urban industry emissions, Beijing and Xianghe sites are also influenced by dust particles originated from the Gobi-Taklamakan deserts. Therefore, they are characterized by the mixed aerosol type. Since the local anthropogenic emissions at Boulder site are not influential as compared to external sources (e.g., forest fires), the main aerosol type for Boulder site is known as continental aerosol type.

2.2. Time series analysis

The null hypothesis for time series modeling using the ARIMA model here is that AOD variations and future trends can be simulated and predicted by the ARIMA model, and the alternative is that the ARIMA model lacks the ability to capture AOD profiles and thus is incapable of forecasting future AOD values. One of the most commonly used ARIMA models is the Box-Jenkins ARIMA model (Box and Jenkins, 1970). For a stationary AOD time series, whose mean and variance remain constant over time, an autoregressive moving average (ARMA) model is adequate to describe the variability. The ARMA model in its formula is a combination of the autoregressive (AR) model with p-order and the moving average (MA) model with q-order, which can be abbreviated as ARMA (p, q) and written as:

$$\phi_p(B)(y_t - \mu) = \theta_q(B)\varepsilon_t \tag{2}$$

where y_t is the observed AOD value at time t; μ is the mean value of y_t; B is the backshift operator and $By_t = y_{t-1}$, $B^2y_t = BBy_t = By_{t-1} = y_{t-2}$, …, $B^k y_t = y_{t-k}$; $\phi_p(B)$ is AR polynomial in B of degree p and $\phi_p(B) = 1 - \phi_1 B - \phi_2 B^2 - \ldots - \phi_p B^p$, $\theta_q(B)$ is MA polynomial in B of degree q and $\theta_q(B) = 1 + \theta_1 B + \theta_2 B^2 + \ldots + \theta_q B^q$; ε_t is the random shocks and $\varepsilon_t \backsim WN(0, \sigma^2)$.

For a non-stationary AOD time series, a differencing process is required till it satisfies the stationary condition. A non-stationary time series can be converted into a stationary ARMA model after d-th differencing, which is defined as ARIMA (p, d, q) and is given by:

$$\phi_p(B)\left((1-B)^d y_t - \mu\right) = \theta_q(B)\varepsilon_t \tag{3}$$

To check whether an AOD series is stationary or not, the

autocorrelation function (ACF) and partial autocorrelation function (PACF) can be applied to the original time series data. ACF (k) describes the AOD correlation at time point t and lagged time point $t-k$. Differencing is considered to be necessary for a time series if there is a slow decay in the behavior of its ACF plots. The PACF (k) describes the same kind of correlation after the effect of all intervening lags is removed. Meanwhile, the ACF and PACF plots can be used to determine plausible values of p, d, and q. The best fitted model is determined by checking the model adequacy (Schwert, 1989) as well as model section criteria such as goodness of fit. Finally, the best fitted model is used to forecast AOD values of 1-year lead-time. The workflow diagram of ARIMA model is shown in Fig. 2.

2.3. Statistical analysis and model validation

2.3.1. Evaluation of original data

Before running the time series model, the quality of AOD data is assessed by performing linear regression analysis for MODIS AOD with respect to AERONET AOD. In addition, Root Mean Square Error (RMSE), Mean Absolute Error (MAE), and Root Mean Bias (RMB) are also used to assess possible MODIS AOD biases compared to AERONET. These evaluation criteria altogether measure the precision, uncertainty, accuracy and bias between the satellite retrievals and ground observations. More detailed information about the evaluation criteria could be found in Bibi et al. (2015). Note that the RMB is computed using the ratio of mean MODIS AOD to mean AERONET AOD. The MODIS AOD is considered to be underestimated as compared to AERONET AOD if $RMB < 1$, and vice versa. The reliability of the data is evaluated via the two-sample independent t-test, which determines whether the sample mean difference in AOD is a real difference between the two populations or merely caused by sampling errors. The null hypothesis is that there is no difference between MODIS and AERONET mean AOD values.

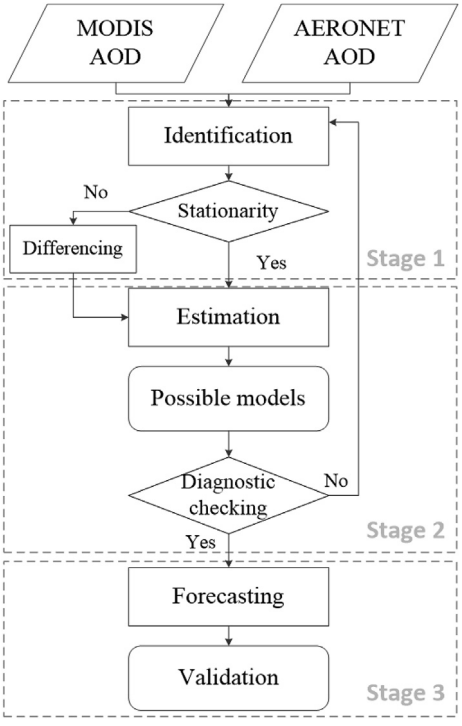

Fig. 2. Flow chart of using ARIMA model to forecast future AOD values.

2.3.2. Validation of ARIMA model

The fitting accuracy of the models (see Stage 2 in Fig. 2) is assessed based on the following statistical metrics: R^2, adjusted R^2, RMSE, MAE, and Mean Absolute Percentage Error (MAPE), referred to R^2, adjusted R^2, RMSE_fit, MAE_fit, and MAPE_fit. In addition, the Bayesian Information Criterion (BIC) is utilized as a measure of goodness-of-fit (Schwarz, 1978). A negative value of BIC means that the model is strongly influenced by the AOD data type (i.e MODIS vs AERONET). All of the aforementioned criteria can reveal the model's capability in simulating the total variance of the AOD series. The better fitted model should be the one that has lower values in RMSE_fit, MAE_fit, MAPE_fit, and BIC but higher values of R^2 and adjusted R^2. Another verification method to assess the goodness-of-fit of a model is to investigate its residuals. The model can be assumed to be a good model if the residuals are not autocorrelated. This can be checked by examining the residuals' ACF and PACF plots, which should have values lying within the 95% critical bounds. In addition, the residuals should bear a resemblance to independent noise with a mean of zero and a constant variance. This can be investigated by checking the frequency distribution of the residuals or by using a quantile-quantile (Q-Q) plot. Apart from looking at residuals' correlations at individual lags, the estimated models can be also evaluated by using Ljung-Box statistics (Ljung and Box, 1978) to account for their combined magnitudes.

The accuracy of the model prediction (see Stage 3 in Fig. 2) is validated using observed AOD values during the year of 2016. Statistical metrics of RMSE, MAE, and MAPE, referred to RMSE_pred, MAE_pred, and MAPE_pred, respectively, are used for this purpose. Note that for the Xianghe site, since the AERONET Level 2.0 AOD is not available in 2016, the Level 1.5 is considered as an alternative. It should be mentioned that the AERONET Level 2.0 AOD data is not complete for 2016 (it is available only for the first seven months of 2016 for MDSC, Boulder, and Beijing sites, and only for the first six months of 2016 for CKU site at the time to process the data). But this problem should not have much impact on our results.

3. Results

3.1. Comparison of MODIS C6 results to AERONET observations

Validation of AOD data retrieved from MODIS C6 was performed against AERONET data over the six sites, as shown in Fig. 3. The computed statistical metrics are summarized in Table 2. In general, best agreements between MODIS and AERONET AODs are found for the GSFC site, followed by MDSC and CKU sites, while relatively poor correlations are found for Xianghe, Beijing, and Boulder sites. However, it should be noted that MODIS and AERONET AODs at all sites are positively correlated, indicating consistency between the two data sets. The lowest values of RMSE and MAE are found for GSFC site whereas the largest values are found for Beijing site. Overestimation of MODIS retrievals is observed across all other sites except for CKU site, as indicated by the RMB values.

Table 3 shows the results derived from two sample independent t-test. It can be seen that all sites other than CKU have a significant level of 0.01 for the t-test, indicating that the null hypothesis should be rejected. Hence, the MODIS and AERONET AOD means are regarded to be from different populations at most sites.

3.2. Monthly, seasonal and annual AOD variability and its primary contributors

Fig. 4 displays the long-term variations of MODIS and AERONET monthly mean AOD data at the six sites. In general, the seasonality is clear and repeatable for GSFC and MDSC data sets while no clearly visible pattern at Beijing and Xianghe can be observed for

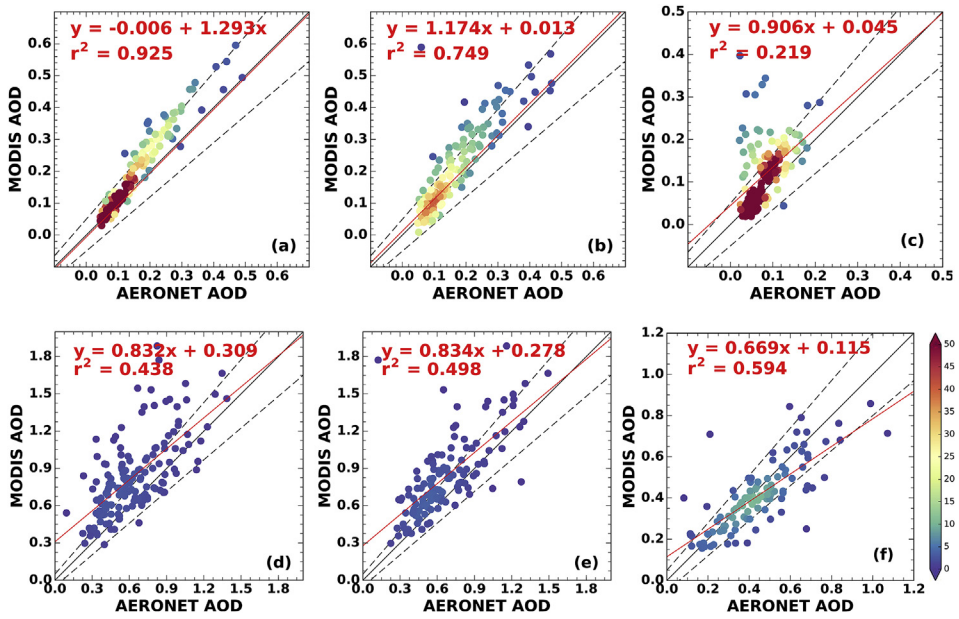

Fig. 3. Comparison of MODIS C6 AOD against AERONET AOD measurements over the six sites. The first row is for ground sites in North America: (a) GSFC, (b) MDSC and (c) Boulder. The second row is for ground sites in East Asia: (d) Beijing, (e) Xianghe and (f) CKU. AERONET AOD has been interpolated to the wavelength of 550 nm. The 1:1 line and the expected errors of ± (0.05 + 15%) are plotted with black solid line and dashed lines, respectively, while the red solid line represents the linear regression result. The ranges of the axes in each plot are different. (For interpretation of the references to colour in this figure legend, the reader is referred to the Web version of this article.)

Table 2
Validation of MODIS C6 AOD against AERONET AOD.

Sites	# of matched months	RMSE	MAE	RMB
GSFC	156	0.057	0.041	1.253
MDSC	144	0.079	0.052	1.254
Boulder	144	0.077	0.047	1.476
Beijing	148	0.316	0.237	1.319
Xianghe	130	0.282	0.197	1.253
CKU	107	0.124	0.087	0.928

Table 3
Results of the sensitivity analysis using two sample independent *t*-test.

Sites	Measurement	*t*-test for equality of means				
		t	df	Sig.(2-tailed)	Mean Difference	Std. Error Difference
GSFC	AERONET MODIS	−3.055	310	0.002	−0.038	0.012
MDSC	AERONET MODIS	−2.669	298	0.008	−0.036	0.013
Boulder	AERONET MODIS	−5.086	297	0.000	−0.036	0.007
Beijing	AERONET MODIS	−5.935	302	0.000	−0.195	0.033
Xianghe	AERONET MODIS	−4.775	284	0.000	−0.166	0.035
CKU	AERONET MODIS	2.251	261	0.025	0.047	0.021

both MODIS and AERONET AODs. Seasonality is relatively evident for Boulder AERONET AOD while extreme MODIS AOD values tend to weaken the pattern. By contrast, the AOD seasonality at CKU is relatively apparent for MODIS data as compared to AERONET data, and the seasonality of AERONET data is apt to diminish due to the scarcity of ground measurements.

Fig. 5 shows annual, seasonal, and monthly mean MODIS and AERONET AODs and the corresponding AEs for the six sites. The AE parameter derived from AERONET was used to help in understanding the dominant sources (coarse- or fine-mode aerosols) that contribute to aerosol discrepancies (García et al., 2012; Li et al., 2014). As can be seen in Fig. 5, profiles of AOD variations in the three different timescales reveal very interesting patterns for these sites.

In general, the annual mean AODs exhibit consistent trends for GSFC, Beijing, and Xianghe sites with some minor differences between MODIS and AERONET AODs. By comparison, the annual mean AOD patterns present varying or even reverse trends for some years at MDSC site, but they still show an overall coherent AOD behaviors. For Boulder site, MODIS AOD fluctuates a lot over time since it is more sensitive to extreme weather conditions. The tendency is not obvious for CKU site due to the lack of sampling data.

The summer season has the highest mean AOD values for the five sites located at mid-latitudes of NH (GSFC, MDSC, Boulder, Beijing, and Xianghe). The high AOD mean values in the season are associated with high values of AE, implying that the major contributor is fine pollution aerosols. But for the site located at CKU, the season with the highest mean AOD is found in spring, accompanied by a little bit higher AE values, implying that the impact of fine-mode aerosols. In fact, various studies have proved that high AOD values in Taiwan during springtime are caused by long transport of pollutants from Asian under the northeasterly winter monsoon (Lin et al., 2007), consistent with our results. On the other hand, the summer season has the lowest mean AOD values for CKU site, and autumn or winter for other five sites. The onset of the summer East Asian Monsoon in May and June, which is concurrent with the rainy season (Kim et al., 2007), probably has a prominent influence on the AOD at CKU site. The precipitation increases the wet removal of aerosols and leads to the decreases in AOD. But for sites in the mid-latitudes of NH, the meteorological and weather conditions during the autumn and wintertime are favorable for the dispersion of the aerosols (Hand et al., 2012; Kim et al., 2007). The relatively high mean AOD in autumn for CKU site may be explained by potential anthropogenic emissions (Hsiao et al., 2017).

It is noteworthy that the monthly mean values of AE generate a

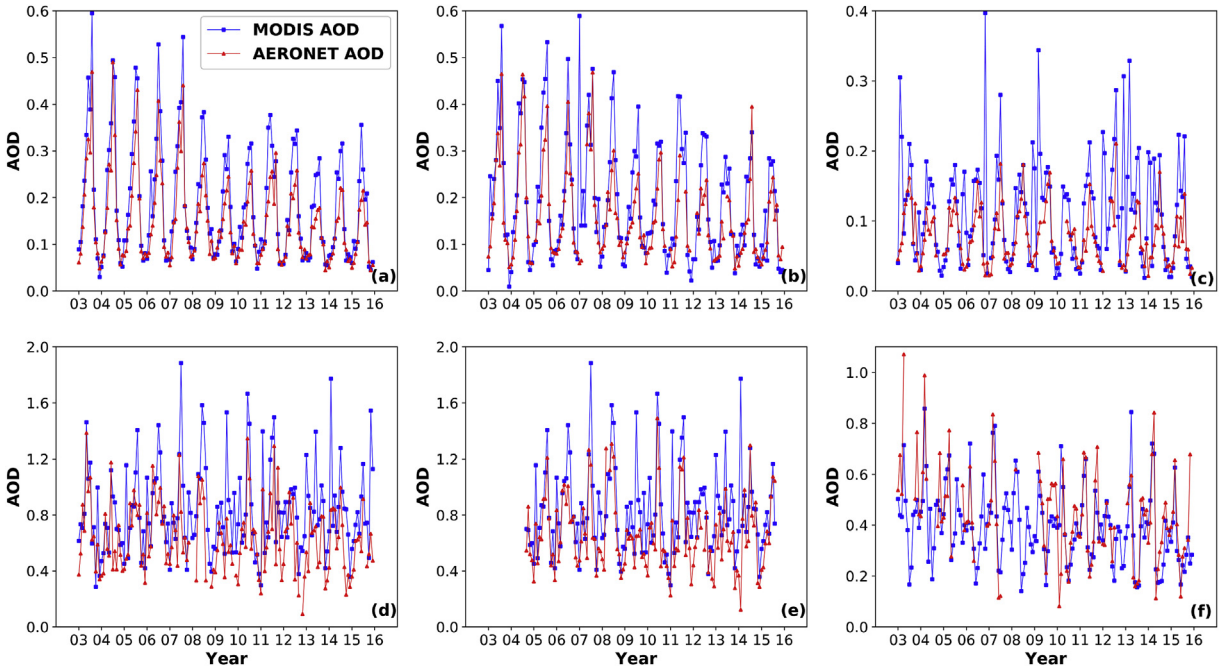

Fig. 4. Monthly mean variations of the MODIS and AERONET AOD data at the six selected sites: (a) GSFC, (b) MDSC, (c) Boulder, (d) Beijing, (e) Xianghe and (f) CKU during the period of Jan 2003–Dec 2015.

similar pattern for the sites in the mid-latitudes NH, suggesting the sources affecting these sites are similar. But it should be noted that the AE values in February at Beijing and Xianghe sites exhibit a decreasing trend, and consequently resulting in a spike of AOD owing to the occurrence of Asian dust. The high values of AOD in March through April at CKU site are associated with the occurrence of large-size dust particles, as evidenced by the relatively declining values of AE (Kim et al., 2007). Besides dust particles, the highest AOD values in March and April for CKU site are also related to long-range transport of agricultural biomass burning from Southeast Asia, which typically occurs in spring. In addition, our results support the results produced by Kim et al. (2007) who reported a monthly mean AOD climax in June and July for Beijing and Xianghe sites and the lowest value during December and January. Similarly, the monthly mean AOD values reach their peaks in July and August for sites in NA. This is partly due to the emission of the anthropogenic fine particles (as indicated by high values of AE), especially sulfate aerosols, which is positively correlated to temperature and reaches maximum values in summer (Saunders and Waugh, 2015). However, compared with GSFC and MDSC sites, Boulder site is dominated by coarse-mode particles with low AE values all the year round. The results from Chin et al. (2007) showed that dust storm can transport from Asia and Africa all the way into western NA, and such things occur more frequently in spring.

3.3. Annual AOD trends and primary causes

The annual AOD trends and associated uncertainties at the six sites are described in Table 4. The Analysis Of Variance (ANOVA) was used to test statistical significance of the annual trends. For example, a *p*-value less than 0.05 indicates that the trends are statistically significant at the 95% confidence intervals. At GSFC and MDSC sites, a decreasing trend at the magnitude of around −0.007 yr^{-1} (at a significance level of 95%) is detected, whereas at Boulder site, a decreasing trend of −0.001 yr^{-1} (at a significance level of 90%) is obtained. The negative tendency is consistent with the annual trend data in many studies in literature: for example, -0.0008 ± 0.0017 yr^{-1} for SeaWiFS and -0.0039 ± 0.0012 yr^{-1} for AERONET at GSFC site from 1997 to 2010 (Hsu et al., 2012); −0.0083 yr^{-1} for MODIS C5 and -0.0079 yr^{-1} for AERONET at MDSC site from 2003 to 2013 (Zhang et al., 2016); and −0.0003 yr^{-1} for MODIS C5 and -0.00004 yr^{-1} for AERONET at Boulder site from 2001 to 2009 (de Meij et al., 2012). This behavior is largely attributed to the decreasing trend of industrial emissions in the US. The Clean Air Act (CAA) controls have successfully reduced air pollution emissions in the US since 1990, especially the emissions of SO_2 and NO_x (Streets et al., 2006). Since industrial activities mainly concentrate on eastern US, the reduction in air pollution emissions is relatively large at GSFC and MDSC sites.

The annual AOD mean values at Beijing site during the studied period exhibit a slight decreasing trend for AERONET (-0.0087 ± 0.0048 yr^{-1}) at a significance level of 90%, while no significant trend is observed in terms of MODIS (0.0053 ± 0.0044 yr^{-1}). Ma et al. (2017) generated similar results. Interestingly, the trend for MODIS becomes obvious from 2006 to 2015 (-0.0042 ± 0.0054 yr^{-1}). This is likely due to the enforcement of the 11th through 12th Five-Year Plan (2006–2010, 2011–2015) that encouraged energy conservation, emission reduction and cleaner production, aiming to mitigate critical air pollution issues in China such as the SO_2, NO_x, fine particles and CO_2 emissions (Feng and Liao, 2016). No significant AOD trends are found for both AERONET and MODIS at Xianghe site, similar to that reported in Li et al. (2014). It seems that these policies did not have much influence on the Xianghe site. However, CKU site shows a negative trend of −0.0172 yr^{-1} for AERONET and −0.0093 yr^{-1} for MODIS at a significance level of 95%, which agrees with the results of Provencal et al. (2014). This is probably attributed to the Air Pollution Control Act (APCA) that promotes renewable energy and green consumption. Under the authorization of APCA, the criteria air pollutants have first been included in the Ambient Air Quality Standards in 1992 (Tsai and Chou, 2005).

3.4. Time series analysis using ARIMA

The capability of ARIMA model in simulating and predicting AOD

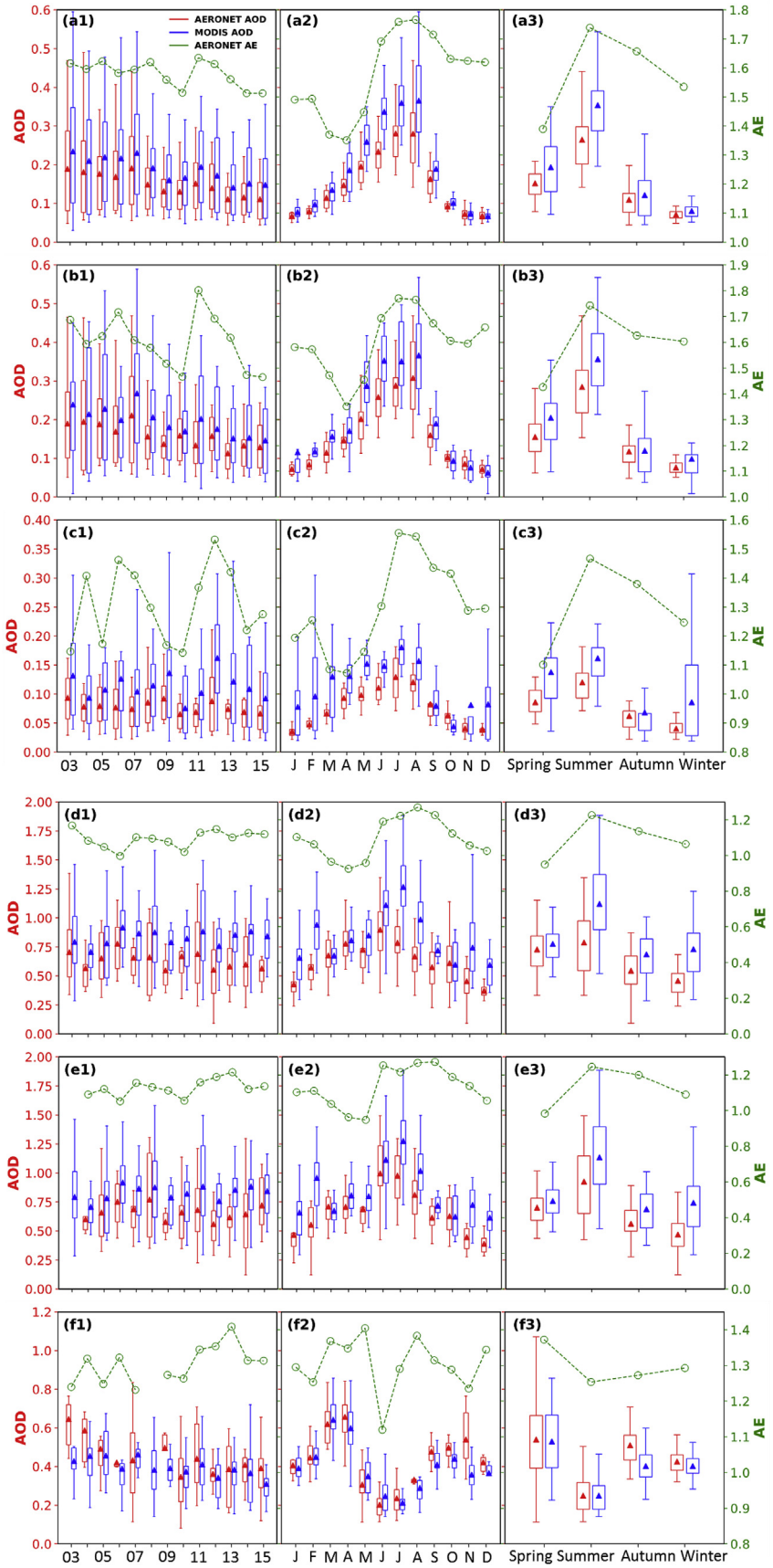

Fig. 5. Annual (left column), monthly (middle column), and seasonal (right column) AOD mean values with regard to MODIS AOD data (blue line) and AERONET AOD data (red line) along with the corresponding Ångström exponent (AE, shown as green line) for the site of GSFC (a*), MDSC (b*), Boulder (c*), Beijing (d*), Xianghe (e*), and CKU (f*), in which * represents 1, 2, and 3, respectively. (For interpretation of the references to colour in this figure legend, the reader is referred to the Web version of this article.)

Table 4
Annual trends and associated uncertainties of AODs for MODIS C6 and AERONET between 2003 and 2015.

Sites	AERONET		MODIS C6	
	Trend (AOD/yr)	Uncertainty	Trend (AOD/yr)	Uncertainty
GSFC	−0.0069[a]	0.0010	−0.0074[a]	0.0012
MDSC	−0.0064[a]	0.0013	−0.0077[a]	0.0016
Boulder	−0.0012[b]	0.0006	−0.0002	0.0017
Beijing	−0.0087[b]	0.0048	0.0053	0.0044
Xianghe	−0.006	0.0064	-9E-05	0.0050
CKU	−0.0172[a]	0.0045	−0.0093[a]	0.0021

The time period for Xianghe is from 2005 to 2015, because data are not available for 2003 and most months of 2004.
[a] Significant at 95%.
[b] Significant at 90%.

time series was analyzed over the six sites. Firstly, the stationarity of the series with the aid of ACF and PACF graphs was used to investigate the autocorrelation of the original data. For example, if the graph of ACF exhibits a cut-off after lag q, the time series is likely to be processed by an ARIMA (0,0,q) or MA(q). However, if the graph of PACF displays a cut-off after lag p, the time series is likely to be processed by an ARIMA (p,0,0) or AR(p). If the original AOD series were identified as nonstationary, it would be transformed to a stationary one by taking d-th differencing of data. In the next stage, the best orders for ARIMA model were determined by examining the ACF and PACF residuals as well as other tests mentioned in Section 2.3.2. The results of diagnostic checking for the best fitted ARIMA models are shown in Fig. S1 – S3 in the Supplementary Material. The residuals at most, if not all (e.g., AERONET AOD at CKU, MODIS AOD at Beijing and Xianghe), sites are approximately normally distributed and therefore implying a good fit of the models.

The statistics for assessing the fitting accuracy of the most suitable models are summarized in Table 5. The site of GSFC has the highest adjusted R^2 (or R^2), followed by MDSC, Boulder/CKU, Xianghe and Beijing sites. Based on the statistical measurement of RMSE_fit, ARIMA models achieve better performance at relatively clean sites (GSFC, MDSC, and Boulder), as indicated by the lower RMSE_fit values. On the contrary, relatively high values of AOD at Beijing and Xianghe sites have relatively high values of RMSE_fit (around 0.2). The RMSE_fit values at CKU site are moderate. However, the relatively high RMSE_fit for AERONET AOD is noticeable partly due to the lack of ground data to fit the model. The MAE_fit displays a consistent pattern with RMSE_fit, despite that it gives the same weight to all errors. On the other hand, the MAPE_fit shows large errors for Boulder MODIS and CKU AERONET, and this implies that large absolute errors existed between certain kinds of simulated and observed AOD values. Negative BIC values are obtained over GSFC, MDSC, Boulder, and CKU sites while positive ones are acquired at other relatively polluted sites.

Results of the best fitted ARIMA model presented in Table S1 reveal the same model for MODIS and AERONET AODs at GSFC and MDSC sites, indicating similar trends and patterns of AOD time series at these two sites. This also confirms a good correlation between MODIS and AERONET AODs. For Boulder site, the regression of AODs relies on data in previous two months and MODIS AOD has more noise that needs to be filtered from fluctuations. An identical behavior is observed for the AERONET AOD at Beijing and Xianghe sites, demonstrating the AOD patterns for these two sites are similar, despite different AOD values. Moreover, longer time series tends to introduce more noise based on best-fitted ARIMA model type for MODIS AOD at Beijing and Xianghe sites. A unique ARIMA model is obtained for data at CKU site, probably due to its geographic location. An interesting phenomenon could be observed that the satellite-derived AOD possesses more noise than ground-based AOD. The Ljung-Box test results for the residuals of the best fitted models indicate that all the p-values (for the selected lag-numbers) are well above 0.05, implying that the residuals are mostly white-noise with little correlation.

Validation of the predicted AOD values in 2016 against the actual values is presented in Table 6. The model performance is evaluated based on RMSE_pred, MAE_pred and MAPE_pred. In general, AERONET AOD has the smallest RMSE_pred, MAE_pred, and MAPE_pred for all sites except CKU. As aforementioned, AERONET AOD at CKU site has the uncertainty problem caused by insufficient data sampling and missing data. In addition, it is evident that the MAPE_pred for MODIS AOD at Boulder site almost reaches 100%, which may result from biases in MODIS AOD products caused by topography, climatology, and surface characteristics (Kahn et al., 2010). The scatterplots of the predicted AODs against the actual AODs values at the six selected sites are provided in Fig. S4. On one hand, the high R^2 values for both MODIS and AERONET AODs indicate the strong predictive power of the models. On the other hand, the ARIMA model cannot predict the extreme AOD values accurately, and consequently may underestimate the AOD values (Soni et al., 2016). This drawback has more influence on MODIS data than on AERONET data. Nevertheless, the null hypothesis that the ARIMA model is capable to simulate and forecast AOD patterns holds true for most sites used in our study.

Fig. 6 shows the relationship among adjusted R^2, RMSE_fit, RMSE_pred and the correlation coefficient (R) between MODIS and AERONET AOD data. Visually, the performance of the ARIMA model is somewhat consistent with the accuracy of the original data used. In general, the fitted and predicted models for AERONET AOD are better than those for MODIS AOD, indicating relatively better quality of AERONET AOD data. Specifically, the high quality of data as indicated by R at GSFC and MDSC sites tend to have high RMSE_fit and RMSE_pred, while relatively low quality of data at Beijing and Xianghe sites tend to have low RMSE_fit and RMSE_pred. However, it is noted that the worst data quality for Boulder site doesn't generate the worst fitting and predicting accuracies, both for MODIS and AERONET AODs. This is partly because in addition to the quality of data, the data values also play an important role in controlling the model performance. For CKU site, the fitting and predicting accuracies of MODIS data are higher than that of AERONET data, implying the limitation of AERONET data.

The fitted and predicted AOD time series are shown in Fig. 7. Overall, the AOD values simulated by the models agree well with the actual values for most sites, with small-AOD values yielding more satisfactory results. The observed values of 2016 fall within the 95% confidence level for sites of GSFC and MDSC. The seasonal patterns of the AOD series are well reproduced (e.g., GSFC, MDSC, and CKU MODIS), as indicated by the periodic variations of observed and simulated data. This reveals the models' capability in predicting reliable AODs at sites with regular annual variations and no significant extreme values. However, given the presence of fluctuations in the data, it is hard to find a perfectly fitted model. This is especially true for Beijing, Xianghe, and Boulder sites where simulations do not correspond well to observations due to the extreme AOD values. In most cases, the models underestimate AOD values, similar to the study results of Soni et al. (2014).

4. Discussion

4.1. Potential sources of aerosol difference for nearby sites

Geographically, sites of GSFC and MDSC (located in two nearby grid cells in the satellite image) and sites of Beijing and Xianghe (located within one grid cell in the satellite image) are two pairs of

Table 5
Fitting statistics of the best fitted ARIMA models for MODIS and AERONET AOD time series data at the six selected sites.

Statistic	GSFC		MDSC		Boulder		Beijing		Xianghe		CKU	
	AERONET	MODIS	AERONET	MODIS	AERONET	MODIS	AERONET	MODIS	AERONET	MODIS	AERONET	MODIS
R^2	0.812	0.839	0.793	0.659	0.649	0.468	0.361	0.270	0.455	0.296	0.514	0.626
Adjusted R^2	0.810	0.838	0.792	0.657	0.646	0.464	0.356	0.265	0.451	0.291	0.509	0.624
RMSE_fit	0.040	0.050	0.044	0.076	0.023	0.055	0.204	0.269	0.198	0.264	0.130	0.098
MAPE_fit	22.030	24.531	25.126	48.746	23.242	59.481	29.994	27.780	27.775	27.547	33.162	20.824
MAE_fit	0.029	0.037	0.033	0.058	0.017	0.040	0.157	0.208	0.159	0.208	0.097	0.070
BIC	−455.44	−383.71	−307.97	−209.59	−638.74	−316.34	12.54	86.15	10.44	68.31	−32.43	−157.48

Table 6
Validation of the predicted and the observed values of AOD for the year 2016 using the best fitted models.

Sites	Measurements	RMSE_pred	MAE_pred	MAPE_pred
GSFC	AERONET	0.031	0.020	21.238
	MODIS	0.043	0.028	21.592
MDSC	AERONET	0.039	0.033	27.033
	MODIS	0.056	0.042	51.906
Boulder	AERONET	0.027	0.023	43.007
	MODIS	0.090	0.066	96.058
Beijing	AERONET	0.274	0.247	59.414
	MODIS	0.293	0.215	30.628
Xianghe	AERONET	0.210	0.161	31.611
	MODIS	0.333	0.257	37.595
CKU	AERONET	0.176	0.153	64.124
	MODIS	0.132	0.096	31.825

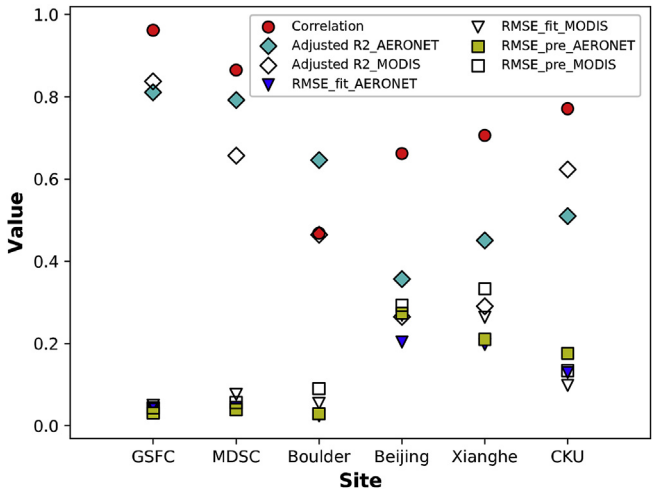

Fig. 6. The relationship between both model fitting and predicting accuracies and the quality of original data.

closely-located sites. This unique feature provides opportunities for a detailed examination of the sources that impact nearby sites without the influence of geographic differences. Table 7 shows the statistical results, based on different metrics, of the two pairs in nearby sites: GSFC and MDSC sites, Beijing and Xianghe sites, respectively. It is observed for both AERONET and MODIS datasets that the annual mean AOD value at MDSC site is greater than that at GSFC site despite that they have the same median (not shown in the table). Moreover, although both sites have the same aerosol type, AODs at MDSC site exhibit more variations as compared to GSFC site. The finding is consistent with the result of earlier study by Chu et al. (2015). The relatively higher annual mean and variance is probably due to its land cover types. The MDSC site is located in Baltimore's Inner Harbor characterized by higher impervious surface (6.521 for MDSC site versus 3.140 for GSFC site as shown in NLCD 2011 (Homer et al., 2015) impervious areas averaged within the corresponding AOD grid cell) and lower vegetation cover, compared with the land cover situation at GSFC site which is surrounded by more forests. The relatively higher AE, on the other hand, confirms the larger impact of fine particles on MDSC site.

The annual mean and variance of AODs at Beijing site are relatively lower than those at Xianghe site, consistent with previous studies (Xia et al., 2016). The relatively small mean and variance of AE at Beijing site imply the existence of coarse particles, which agrees with the finding of Cheng et al. (2006). The relatively high mean and variance of AE at Xianghe site might be attributed to the regional impact of Hebei Province. The AOD and AE difference between Beijing and Xianghe sites is small in winter (0.0005) as shown in Table 8, indicating that the sources (e.g., fossil fuel combustion and biomass burning) for these two sites are probably the same during the wintertime. However, their AOD values have a big difference in summer, despite the fairly small difference in AE. In spring, the mean AOD value at Beijing site is 1.77% larger than that at Xianghe site. This is probably due to prominent influence of dust storm, inferred from the smaller AE at Beijing site. Forests in Xianghe may act as a filter to screen out the coarse-mode aerosols, such as dust storm, outside the region (Tan et al., 2015). Thanks to the launch of Desertification Combating Program around Beijing and Tianjin projects, forest filter effect appears to be evident for Beijing, as indicated by the decrease (increase) of the spring differenced AOD (AE) value from 0.053 (−0.083) during 2005–2007 to −0.003 (−0.026) during 2008–2015. The relatively higher AOD and AE values in fall at Xianghe site might be caused by a large magnitude of biomass burning that usually takes place in densely vegetated areas (Boiyo et al., 2017).

Overall, since effects of the topography and climatology tend to be minimal for nearby sites, the discrepancy in land cover types, especially in vegetation types, plays an important role in the difference of the aerosol characteristics at nearby sites.

4.2. Evaluation of model performance

4.2.1. Accuracy of model prediction

The best model was selected using the nearby sites to minimize external impacts for a contrasting analysis. Huesca et al. (2014) pointed out that remote sensing time series data were usually associated with highly significant seasonal changes of ground features, thus the multiplicative seasonal autoregressive integrated moving average (SARIMA) model should be a better choice. A detailed description of the SARIMA model can be found in Box and Jenkins (1970) and the model's equation is provided in the Supplementary material. In this study, performances of ARIMA models and SARIMA models are evaluated for the two nearby sites. Both fitting accuracy and predicting accuracy are considered for selecting the appropriate model. The evaluation results of the first eight

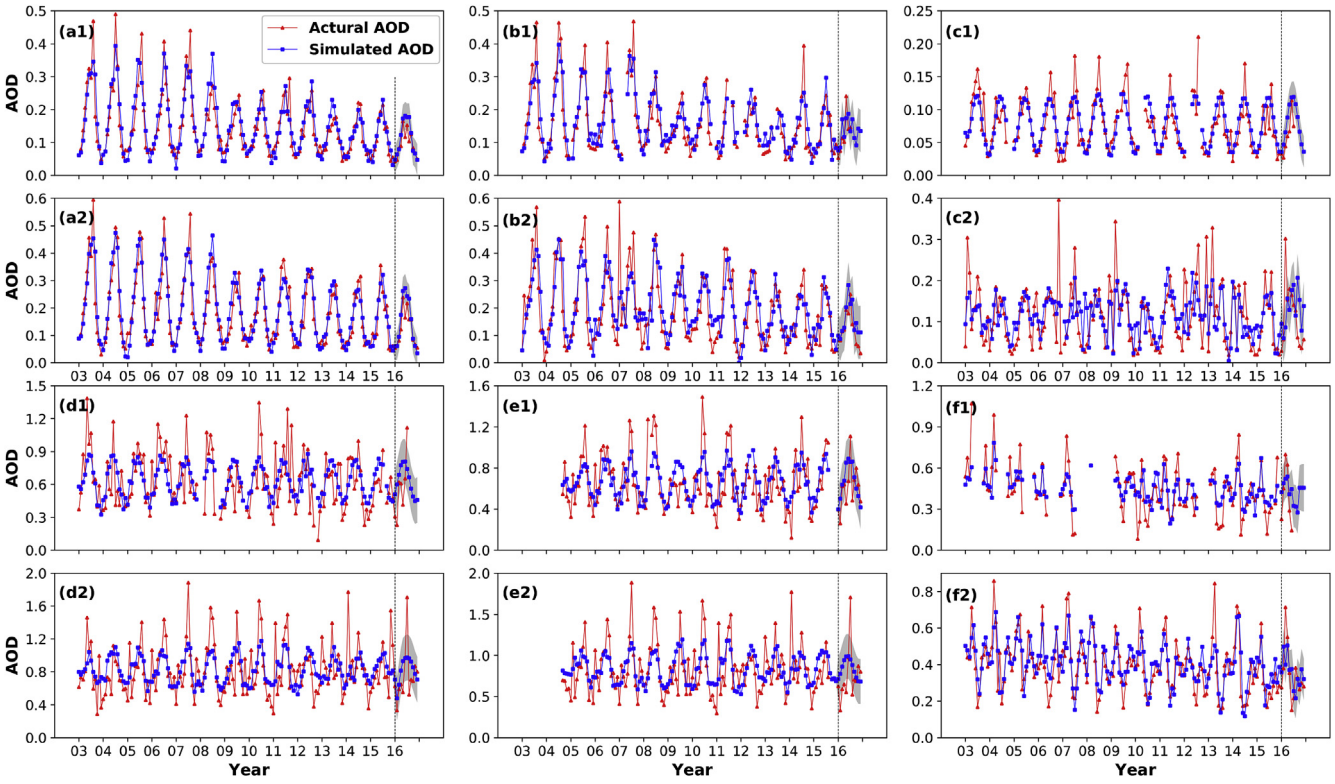

Fig. 7. Time series plots of the actual AOD values (red line) and the simulated values (blue line) for site of GSFC (a*), MDSC (b*), Boulder (c*), Beijing (d*), Xianghe (e*), and CKU (f*). * indicates 1 and 2, in which 1 stands for AERONET AOD and 2 stands for MODIS AOD. The forecast values for the year 2016 are shown at the 95% confidence level (grey shaded area). The vertical black dashed line shows the beginning of the year 2016. (For interpretation of the references to colour in this figure legend, the reader is referred to the Web version of this article.)

Table 7
Statistical comparison results of the AODs and AE at the two pairs of nearby sites during 2003–2015[a].

Sites	AERONET_AOD	AERONET_AE	MODIS_AOD
GSFC	0.150 ± 0.092	1.580 ± 0.169	0.187 ± 0.124
MDSC	0.159 ± 0.097	1.599 ± 0.235	0.195 ± 0.130
Beijing	0.634 ± 0.249	1.083 ± 0.147	0.834 ± 0.312
Xianghe	0.663 ± 0.266	1.130 ± 0.161	0.834 ± 0.312

[a] The time period for Beijing and Xianghe is from 2004 to 2015.

Table 8
Seasonal differences between Beijing and Xianghe sites in terms of AOD and AE during 2005–2015[a].

Season	Difference between Beijing and Xianghe (value at Beijing − value at Xianghe)	
	AERONET_AOD	AERONET_AE
Spring (MAM)	0.0124	−0.0411
Summer (JJA)	−0.1409	−0.0302
Fall (SON)	−0.0106	−0.0700
Winter (DJF)	0.0005	−0.0331

[a] MAM, March–April–May; JJA, June–July–August; SON, September–October–November; DJF, December–January–February.

models with high performance using AERONET and MODIS data are provided in Figs. S5 and S6.

In general, an identical optimal non-seasonal ARIMA model is applied for both MODIS and AERONET at GSFC site after comparing various models through trial and error. The suitable non-seasonal ARIMA models for MDSC site are also the same for both MODIS and AERONET despite that the fitting and predicting accuracies at MDSC site are relatively lower than those at GSFC site. Interestingly, for both GSFC and MDSC sites, the best fitted SARIMA model performs relatively better for MODIS than the non-seasonal ARIMA model (discussed in Section 3.4), while the predicting accuracy of the best fitted SARIMA is not so good as that of the non-seasonal ARIMA model for AERONET. Unlike GSFC and MDSC sites, the pair of Beijing and Xianghe sites share the same AOD grid in the remotely sensed image. Thus, their optimal ARIMA models for MODIS are the same. Compared with non-seasonal ARIMA, the use of SARIMA model for MODIS data has significantly improved the fitting accuracy by 10.3% but reduced the predicting accuracy by 10.2% in terms of RMSE. On the other hand, the accuracy of the non-seasonal ARIMA model is higher for Xianghe AERONET data than that for Beijing AERONET data. Despite the fact that SARIMA has reduced BIC when applied to these two sites, little improvements could be achieved generally.

Overall, more accurate models can be obtained from the time series data that have more distinct seasonal patterns (Jiang et al., 2010). The desirable model may be the one with a combined influence on data quality, reliability, and low-AOD values.

4.2.2. Uncertainties in the model performance

As aforementioned, the quality of the AOD data plays a crucial role in the performance of the ARIMA model. The differences in data quality presumably result from the AOD retrieval algorithms, the geographical features, the climatological characteristics, the land surface conditions, and the heterogeneity with regard to aerosol types (Ichoku et al., 2005; Sayer et al., 2014). On the other hand, possible errors could also exist for ground-measured data, and they may be caused by instrument defects or operational failures. On top of that, ground observations measured at high

elevations are not representative of regional aerosol variations (Ichoku et al., 2005). The high quality of MODIS AOD data at GSFC and MDSC sites is largely attributed to the good retrieval algorithm. These two sites are located in eastern U.S., which is characterized by vegetation, suburban, or urban surfaces over a fairly flat, low-lying area. Consequently, the DT algorithm applied in this region tends to exhibit small bias. It is expected that the ARIMA model can be applicable in the regions where MODIS observations are well correlated with AERONET measurements. However, the retrieved aerosol product is less accurate in western U.S. (e.g., Boulder) than in eastern U.S., due to the complex aerosol formation mechanisms complicated by emissions transported from Asia, widespread bright surfaces, and smoke from wildfires (Yu et al., 2008). Therefore, it is more rational to predict future AOD values using AERONET AOD. In contrast to the Boulder site, the sampling limitation of AERONET AOD at CKU site renders the forecast to rely on MODIS AOD. The heterogeneous urban features and mixed aerosol types at Beijing and Xianghe sites make it hard to accurately predict AOD values in a long term, as indicated by the growing deviations with time between the predicted and actual AOD values (see Fig. 7). But it is feasible to use the ARIMA model for predictions during short-term periods (e.g., 12 months).

Since the ARIMA model is sensitive to extreme AOD values, possible contributors to the abnormal values of AOD are analyzed. For example, Hsu et al. (2012) pointed out that the periodic, abrupt, fluctuations in AOD time series might result from natural phenomena such as large-scale climatic conditions associated with El Niño Southern Oscillation (ENSO) events. In order to examine how inter-annual variability of AOD at the six sites might be potentially influenced by ENSO, the Multivariate ENSO Index (MEI; Wolter and Timlin (1998), accessible at https://www.esrl.noaa.gov/psd/enso/mei/) was adopted from Jan. 2003 to Dec. 2015. The time series of deseasonalized monthly AOD anomalies and MEI during the study period are illustrated in Fig. S7. The peaks of AOD abnormal values are consistent with the high ranked El Niño events but with certain time lags, implying that the ENSO year could result in abnormal high/low values in AOD. A further quantitative study on the correlation between monthly AOD anomaly and MEI, and correlation between monthly AE anomaly and MEI is conducted. Considering the whole time span, there is indeed no significant correlation between monthly AOD anomaly and MEI. This result is consistent with the finding of Li et al. (2011). The correlation coefficients between monthly AE anomaly and MEI at a significant level of 95% are −0.202, −0.196, and 0.227 for GSFC, MDSC, and Boulder sites, respectively. No significant correlation was found between monthly AE anomaly and MEI for the other three sites. Furthermore, a time lag analysis between the correlation of MEI and AOD/AE anomaly is performed and provided in Fig. S8. It is observed that the correlation between MEI and aerosol properties (e.g, AOD and AE) is not so representative, probably because a 13-year period of aerosol records is still relatively short for understanding large-scale climatic influence of phenomenon like ENSO (Kärner, 2002). A longer historical timescale would be better for the prediction of AOD and the analysis of its relationships with large scale climatic elements.

4.2.3. Sensitivity of the model performance

The missing aerosol data can be one of the major concerns for the use of the AOD data in application studies, such as epidemiology. Therefore, the impact of the missing AOD data on the performance of ARIMA model was examined. The GSFC site was selected for simulation due to its data completeness during the study period. 2%–50% of AOD data were randomly removed from both MODIS and AERONET time series, and the analysis results are shown in Fig. 8. For AERONET AOD data, the fitting accuracy, as represented by R^2, Adjusted R^2, RMSE_fit, MAE_fit, and MAPE_fit indices (in solid lines) first remains stable and then slightly increases, for around 26% of missing data. However, the predicting accuracy, represented by RMSE_pred, MAE_pred, and MAPE_pred indices (in dashed lines) decreases at this point. A similar behavior is found for MODIS AOD, with around 22% of missing data,

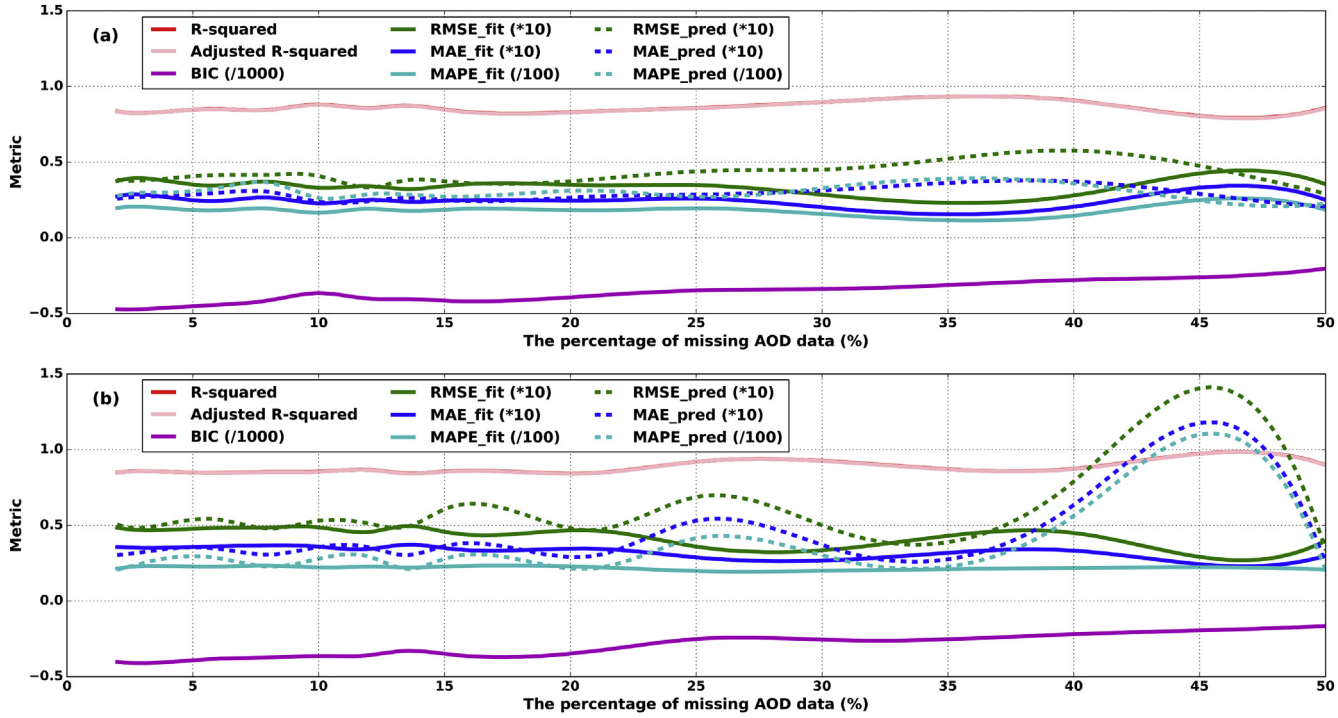

Fig. 8. Analysis of the relationships between the performance of the ARIMA model and the percentage of the missing AERONET AOD data (a), and the missing MODIS AOD data (b). The fitting accuracy of the model is represented by solid lines while the predicting accuracy is represented by dashed lines.

indicating a trade-off between fitting accuracy and predicting accuracy. The BIC, however, shows a steadily positive trend as the amount of missing data increases. The precision of the model is not significant when the proportion of missing values exceeded 50% for AERONET AOD and 40% for MODIS AOD. Interestingly, a consistent pattern of metrics is observed for MODIS AOD, suggesting some intrinsic noises in the AOD time series. Nevertheless, this phenomenon is not evident for AERONET AOD. In addition, the fluctuation of MODIS time series is relatively greater than that of AERONET, suggesting that MODIS AOD is more sensitive to the missing data. In general, the performance of the ARIMA model is less vulnerable to the missing AOD values (with a certain percentage range, e.g., 20%) due to the small amplitude caused by growing volume of missing values. However, the model may be subject to a data convergence problem when the number of missing observations increases.

4.3. Implications for climate change mitigation

Based on the above analysis, policy implications are suggested for mitigating aerosol pollution and climate change from the following two aspects.

From the perspective of emission sinks, as indicated by the case studies of nearby sites in Section 4.1, forests acts as dry deposition source to aerosol particles. At the same time, forests also serves as carbon sinks to CO_2 emissions. Given the dual functions of forests, initiative of reforestation should be attached special significance in climate change mitigation (Canadell and Raupach, 2008). For example, the ecological restoration projects in China have collectively offset 9.4% of the nation's fossil fuel CO_2 production during the 2000s (Lu et al., 2018), while forest growth and afforestation in the U.S. counterbalance about 13% of the CO_2 emissions (Vose et al., 2012). Therefore, the government can continually focus on reforestation programs. In the long-term, however, attention should be paid to the carbon saturation issue associated with forests growth (Zhou et al., 2006).

From the perspective of emission sources, as inferred from Section 3.3, policies on emission regulations and cleaner energy have achieved substantial reduction in aerosol emissions. Likewise, climate change mitigation and human health also benefit from these efforts, though the magnitude might be varied by region. For instance, the use of biofuels in the U.S. may offer health benefits from reduced fine particles and climate change benefits from reduced CO_2 emissions relative to fossil fuels. However, the aggressive policy demanding a sharp rise in biofuel production might cancel out these benefits (Hill et al., 2009). On the other hand, even a modest improvement in energy efficiency and air pollution control technology could yield air quality, climate, and health benefits in China (Peng et al., 2017). It is suggested that policy-makers should take the strategy limits and the regional difference into account to coordinate cross influences and maximize sustainable development.

5. Conclusions

In this study, monthly mean satellite AOD data, in conjunction with ground AOD measurements are used to investigate the aerosol trends, prediction, and driving forces at six sites across North America and East Asia during the period of 2003–2015. A sustained downward trend of AOD is observed both for MODIS and AERONET data over sites of GSFC, MDSC and CKU, at 95% significance level. The decreasing trend is also found for AERONET AOD at Boulder and Beijing sites at a significant level of 90%. However, MODIS AODs at Boulder and Beijing sites, and both MODIS and AERONET AODs at Xianghe site reveal negligible trends. Moreover, the results of monthly and seasonal variabilities indicate consistent aerosol variations at sites mainly located in mid-latitudes of northern hemisphere. However, these variations may also be impacted by regional differences in geographic location, climatology, and land cover types.

In addition, the time series ARIMA model is used to predict the future AOD values of MODIS and AERONET in 2016. Based on the features of AOD time series, a set of specific ARIMA models were evaluated. The forecasting results of the non-seasonal ARIMA model show that the model performs better for AERONET AOD than MODIS AOD for all sites except for CKU, which suggests that the predictive power of the model heavily depends on the number of missing data. Furthermore, AOD quality, AOD reliability and low-AOD values have a joint influence on the performance of the ARIMA model. Comparison of the nearby sites reveals that the seasonal ARIMA model outperforms the non-seasonal ARIMA model for time series that presents distinct seasonal patterns.

Because of the simplicity of the ARIMA model, it lacks the capability to completely account for the sudden changes in aerosols such as the influence of large scale climate factor ENSO. In addition, this exploration study is based on the assumption that factors (e.g., land cover types, meteorology) that had influenced the past behaviors of AOD will continuously influence its future behaviors in the same way. But in reality these factors might change over time. Therefore, our future work will focus on improving predictions using Kalman filtering techniques and extending our analysis to cover broader spatial scale. Furthermore, the driving factors will be also considered in the establishment of the time series forecast model to quantitatively explore their contributions to the aerosol variations. The findings would be important for advancing the knowledge of long-term aerosol trend analysis and modeling, which could provide insights into the interplay of aerosol variations, carbon cycle, and climate change. Based on the case studies, it is suggested that the enforcement of regulations on emission sources and the initiative of reforestation on emission sinks could have potential implications for climate change mitigation.

Appendix A. Supplementary data

Supplementary data to this article can be found online at https://doi.org/10.1016/j.jclepro.2019.03.121.

References

Andreae, M.O., Merlet, P., 2001. Emission of trace gases and aerosols from biomass burning. Glob. Biogeochem. Cycles 15 (4), 955–966.
Bibi, H., Alam, K., Chishtie, F., Bibi, S., Shahid, I., Blaschke, T., 2015. Intercomparison of MODIS, MISR, OMI, and CALIPSO aerosol optical depth retrievals for four locations on the Indo-Gangetic plains and validation against AERONET data. Atmos. Environ. 111 (Suppl. C), 113–126.
Boiyo, R., Kumar, K.R., Zhao, T., Bao, Y., 2017. Climatological analysis of aerosol optical properties over East Africa observed from space-borne sensors during 2001–2015. Atmos. Environ. 152, 298–313.
Box, G.E.P., Jenkins, G.M., 1970. Time Series Analysis: Forecasting and Control. Holden-Day, San Francisco.
Brunekreef, B., Holgate, S.T., 2002. Air pollution and health. Lancet 360 (9341), 1233–1242.
Canadell, J.G., Raupach, M.R., 2008. Managing forests for climate change mitigation. Science 320 (5882), 1456–1457.
Casazza, M., Lega, M., Liu, G., Ulgiati, S., Endreny, T.A., 2018. Aerosol pollution, including eroded soils, intensifies cloud growth, precipitation, and soil erosion: a review. J. Clean. Prod. 189, 135–144.
Chen, W.-N., Chen, Y.-W., Chou, C.C.K., Chang, S.-Y., Lin, P.-H., Chen, J.-P., 2009. Columnar optical properties of tropospheric aerosol by combined lidar and sunphotometer measurements at Taipei, Taiwan. Atmos. Environ. 43 (17), 2700–2708.
Cheng, T., Wang, H., Xu, Y., Li, H., Tian, L., 2006. Climatology of aerosol optical properties in northern China. Atmos. Environ. 40 (8), 1495–1509.
Chin, M., Diehl, T., Ginoux, P., Malm, W., 2007. Intercontinental transport of pollution and dust aerosols: implications for regional air quality. Atmos. Chem. Phys. 7 (21), 5501–5517.

Chou, M.-D., Lin, P.-H., Ma, P.-L., Lin, H.-J., 2006. Effects of aerosols on the surface solar radiation in a tropical urban area. J. Geophys. Res.: Atmos. 111, D15207.
Chu, D.A., Ferrare, R., Szykman, J., Lewis, J., Scarino, A., Hains, J., Burton, S., Chen, G., Tsai, T., Hostetler, C., Hair, J., Holben, B., Crawford, J., 2015. Regional characteristics of the relationship between columnar AOD and surface PM2.5: application of lidar aerosol extinction profiles over Baltimore–Washington Corridor during DISCOVER-AQ. Atmos. Environ. 101, 338–349.
de Meij, A., Pozzer, A., Lelieveld, J., 2012. Trend analysis in aerosol optical depths and pollutant emission estimates between 2000 and 2009. Atmos. Environ. 51, 75–85.
Dubovik, O., Smirnov, A., Holben, B.N., King, M.D., Kaufman, Y.J., Eck, T.F., Slutsker, I., 2000. Accuracy assessments of aerosol optical properties retrieved from Aerosol Robotic Network (AERONET) Sun and sky radiance measurements. J. Geophys. Res.: Atmos. 105 (D8), 9791–9806.
Feng, L., Liao, W., 2016. Legislation, plans, and policies for prevention and control of air pollution in China: achievements, challenges, and improvements. J. Clean. Prod. 112, 1549–1558.
French, K.R., Schwert, G.W., Stambaugh, R.F., 1987. Expected stock returns and volatility. J. Financ. Econ. 19 (1), 3–29.
García, O.E., Díaz, J.P., Expósito, F.J., Díaz, A.M., Dubovik, O., Derimian, Y., Dubuisson, P., Roger, J.C., 2012. Shortwave radiative forcing and efficiency of key aerosol types using AERONET data. Atmos. Chem. Phys. 12 (11), 5129–5145.
Garland, R.M., Schmid, O., Nowak, A., Achtert, P., Wiedensohler, A., Gunthe, S.S., Takegawa, N., Kita, K., Kondo, Y., Hu, M., Shao, M., Zeng, L.M., Zhu, T., Andreae, M.O., Pöschl, U., 2009. Aerosol optical properties observed during Campaign of Air Quality Research in Beijing 2006 (CAREBeijing-2006): characteristic differences between the inflow and outflow of Beijing city air. J. Geophys. Res.: Atmos. 114, D00G04.
Gemitzi, A., Stefanopoulos, K., 2011. Evaluation of the effects of climate and man intervention on ground waters and their dependent ecosystems using time series analysis. J. Hydrol. 403 (1), 130–140.
Giles, D.M., Holben, B.N., Eck, T.F., Sinyuk, A., Smirnov, A., Slutsker, I., Dickerson, R.R., Thompson, A.M., Schafer, J.S., 2012. An analysis of AERONET aerosol absorption properties and classifications representative of aerosol source regions. J. Geophys. Res.: Atmos. 117, D17203.
Granger, C.W.J., Newbold, P., 2014. Forecasting Economic Time Series. Academic Press.
Hand, J.L., Schichtel, B.A., Pitchford, M., Malm, W.C., Frank, N.H., 2012. Seasonal composition of remote and urban fine particulate matter in the United States. J. Geophys. Res.: Atmos. 117, D05209.
Hill, J., Polasky, S., Nelson, E., Tilman, D., Huo, H., Ludwig, L., Neumann, J., Zheng, H., Bonta, D., 2009. Climate change and health costs of air emissions from biofuels and gasoline. Proc. Natl. Acad. Sci. Unit. States Am. 106 (6), 2077–2082.
Holben, B.N., Eck, T.F., Slutsker, I., Tanré, D., Buis, J.P., Setzer, A., Vermote, E., Reagan, J.A., Kaufman, Y.J., Nakajima, T., Lavenu, F., Jankowiak, I., Smirnov, A., 1998. AERONET—a federated instrument network and data archive for aerosol characterization. Rem. Sens. Environ. 66 (1), 1–16.
Homer, C., Dewitz, J., Yang, L., Jin, S., Danielson, P., Xian, G., Coulston, J., Herold, N., Wickham, J., Megown, K., 2015. Completion of the 2011 national land cover database for the conterminous United States – representing a decade of land cover change information. Photogramm. Eng. Rem. Sens. 81 (5), 345–354.
Hsiao, T.-C., Chen, W.-N., Ye, W.-C., Lin, N.-H., Tsay, S.-C., Lin, T.-H., Lee, C.-T., Chuang, M.-T., Pantina, P., Wang, S.-H., 2017. Aerosol optical properties at the Lulin Atmospheric Background Station in Taiwan and the influences of long-range transport of air pollutants. Atmos. Environ. 150, 366–378.
Hsu, N.C., Gautam, R., Sayer, A.M., Bettenhausen, C., Li, C., Jeong, M.J., Tsay, S.C., Holben, B.N., 2012. Global and regional trends of aerosol optical depth over land and ocean using SeaWiFS measurements from 1997 to 2010. Atmos. Chem. Phys. 12 (17), 8037–8053.
Huang, J., Kondragunta, S., Laszlo, I., Liu, H., Remer, L.A., Zhang, H., Superczynski, S., Ciren, P., Holben, B.N., Petrenko, M., 2016. Validation and expected error estimation of Suomi-NPP VIIRS aerosol optical thickness and Ångström exponent with AERONET. J. Geophys. Res.: Atmos. 121 (12), 7139–7160.
Huesca, M., Litago, J., Merino-de-Miguel, S., Cicuendez-López-Ocaña, V., Palacios-Orueta, A., 2014. Modeling and forecasting MODIS-based Fire Potential Index on a pixel basis using time series models. Int. J. Appl. Earth Obs. Geoinf. 26, 363–376.
Ichoku, C., Remer, L.A., Eck, T.F., 2005. Quantitative evaluation and intercomparison of morning and afternoon moderate resolution imaging spectroradiometer (MODIS) aerosol measurements from terra and aqua. J. Geophys. Res.: Atmos. 110, D10S03.
IPCC, 2013. Climate Change 2013: the Physical Science Basis. Contribution of Working Group I to the Fifth Assessment Report of the Intergovernmental Panel on Climate Change. Cambridge University Press, Cambridge, United Kingdom and New York, NY, USA.
Jiang, B., Liang, S., Wang, J., Xiao, Z., 2010. Modeling MODIS LAI time series using three statistical methods. Rem. Sens. Environ. 114 (7), 1432–1444.
Kahn, R.A., Gaitley, B.J., Garay, M.J., Diner, D.J., Eck, T.F., Smirnov, A., Holben, B.N., 2010. Multiangle imaging SpectroRadiometer global aerosol product assessment by comparison with the aerosol robotic network. J. Geophys. Res.: Atmos. 115, D23209.
Kärner, O., 2002. On nonstationarity and antipersistency in global temperature series. J. Geophys. Res.: Atmos. 107 (D20), 4415.
Kim, S.-W., Yoon, S.-C., Kim, J., Kim, S.-Y., 2007. Seasonal and monthly variations of columnar aerosol optical properties over east Asia determined from multi-year MODIS, LIDAR, and AERONET Sun/sky radiometer measurements. Atmos. Environ. 41 (8), 1634–1651.
Levy, R.C., Mattoo, S., Munchak, L.A., Remer, L.A., Sayer, A.M., Patadia, F., Hsu, N.C., 2013. The Collection 6 MODIS aerosol products over land and ocean. Atmos. Meas. Tech. 6 (11), 2989–3034.
Li, J., Carlson, B.E., Dubovik, O., Lacis, A.A., 2014. Recent trends in aerosol optical properties derived from AERONET measurements. Atmos. Chem. Phys. 14 (22), 12271–12289.
Li, J., Carlson, B.E., Lacis, A.A., 2011. El Niño–Southern Oscillation correlated aerosol Ångström exponent anomaly over the tropical Pacific discovered in satellite measurements. J. Geophys. Res.: Atmos. 116, D20204.
Li, X., Zhang, C., Li, W., Liu, K., 2017. Evaluating the use of DMSP/OLS nighttime light imagery in predicting PM2.5 concentrations in the northeastern United States. Rem. Sens. 9 (6).
Lin, C.Y., Wang, Z., Chen, W.N., Chang, S.Y., Chou, C.C.K., Sugimoto, N., Zhao, X., 2007. Long-range transport of Asian dust and air pollutants to Taiwan: observed evidence and model simulation. Atmos. Chem. Phys. 7 (2), 423–434.
Liu, Y., Sarnat, J.A., Coull, B.A., Koutrakis, P., Jacob, D.J., 2004. Validation of Multiangle Imaging Spectroradiometer (MISR) aerosol optical thickness measurements using Aerosol Robotic Network (AERONET) observations over the contiguous United States. J. Geophys. Res.: Atmos. 109, D06205.
Ljung, G.M., Box, G.E.P., 1978. On a measure of lack of fit in time series models. Biometrika 65 (2), 297–303.
Lu, F., Hu, H., Sun, W., Zhu, J., Liu, G., Zhou, W., Zhang, Q., Shi, P., Liu, X., Wu, X., Zhang, L., Wei, X., Dai, L., Zhang, K., Sun, Y., Xue, S., Zhang, W., Xiong, D., Deng, L., Liu, B., Zhou, L., Zhang, C., Zheng, X., Cao, J., Huang, Y., He, N., Zhou, G., Bai, Y., Xie, Z., Tang, Z., Wu, B., Fang, J., Liu, G., Yu, G., 2018. Effects of national ecological restoration projects on carbon sequestration in China from 2001 to 2010. Proc. Natl. Acad. Sci. Unit. States Am. 115 (16), 4039–4044.
Ma, Q., Li, Y., Liu, J., Chen, J.M., 2017. Long temporal analysis of 3-km MODIS aerosol product over east China. IEEE J. Select. Topics Appl. Earth Observat. Remot. Sens. 10 (6), 2478–2490.
Meng, J., Liu, J., Guo, S., Li, J., Li, Z., Tao, S., 2016. Trend and driving forces of Beijing's black carbon emissions from sectoral perspectives. J. Clean. Prod. 112, 1272–1281.
Ocko, I.B., Ginoux, P.A., 2017. Comparing multiple model-derived aerosol optical properties to spatially collocated ground-based and satellite measurements. Atmos. Chem. Phys. 17 (7), 4451–4475.
Peng, W., Yang, J., Wagner, F., Mauzerall, D.L., 2017. Substantial air quality and climate co-benefits achievable now with sectoral mitigation strategies in China. Sci. Total Environ. 598, 1076–1084.
Provencal, S., Kishcha, P., Elhacham, E., daSilva, A.M., Alpert, P., Suarez, M.J., 2014. Technical report series on global modeling and data assimilation. In: Estimates of AOD Trends (2002-2012) Over the World's Major Cities Based on the MERRA Aerosol Reanalysis, vol. 32, 2002-2012.
Ramanathan, V., Carmichael, G., 2008. Global and regional climate changes due to black carbon. Nat. Geosci. 1 (4), 221–227.
Saunders, R.O., Waugh, D.W., 2015. Variability and potential sources of summer PM2.5 in the Northeastern United States. Atmos. Environ. 117, 259–270.
Sayer, A.M., Munchak, L.A., Hsu, N.C., Levy, R.C., Bettenhausen, C., Jeong, M.J., 2014. MODIS Collection 6 aerosol products: comparison between Aqua's e-Deep Blue, Dark Target, and "merged" data sets, and usage recommendations. J. Geophys. Res.: Atmos. 119 (24), 13,965–913,989.
Schwarz, G., 1978. Estimating the dimension of a model. Ann. Stat. 6 (2), 461–464.
Schwert, G.W., 1989. Tests for unit roots: a Monte Carlo investigation. J. Bus. Econ. Stat. 7 (2), 147–159.
Shi, H., Wang, Y., Chen, J., Huisingh, D., 2016. Preventing smog crises in China and globally. J. Clean. Prod. 112, 1261–1271.
Soni, K., Kapoor, S., Parmar, K.S., Kaskaoutis, D.G., 2014. Statistical analysis of aerosols over the Gangetic–Himalayan region using ARIMA model based on long-term MODIS observations. Atmos. Res. 149, 174–192.
Soni, K., Parmar, K.S., Kapoor, S., Kumar, N., 2016. Statistical variability comparison in MODIS and AERONET derived aerosol optical depth over Indo-Gangetic Plains using time series modeling. Sci. Total Environ. 553, 258–265.
Streets, D.G., Wu, Y., Chin, M., 2006. Two-decadal aerosol trends as a likely explanation of the global dimming/brightening transition. Geophys. Res. Lett. 33, L15806.
Tan, C., Zhao, T., Xu, X., Liu, J., Zhang, L., Tang, L., 2015. Climatic analysis of satellite aerosol data on variations of submicron aerosols over East China. Atmos. Environ. 123 (Part B), 392–398.
Tie, X., Brasseur, G.P., Zhao, C., Granier, C., Massie, S., Qin, Y., Wang, P., Wang, G., Yang, P., Richter, A., 2006. Chemical characterization of air pollution in Eastern China and the Eastern United States. Atmos. Environ. 40 (14), 2607–2625.
Tsai, W.T., Chou, Y.H., 2005. Overview of environmental impacts, prospects and policies for renewable energy in Taiwan. Renew. Sustain. Energy Rev. 9 (2), 119–147.
Vose, J.M., Peterson, D.L., Patel-Weynand, T., 2012. Effects of Climatic Variability and Change on Forest Ecosystems: a Comprehensive Science Synthesis for the US. Gen. Tech. Rep. PNW-GTR-870, vol. 265. US Department of Agriculture, Forest Service, Pacific Northwest Research Station, Portland, OR, p. 870.
Wang, Y., Sun, M., Yang, X., Yuan, X., 2016. Public awareness and willingness to pay for tackling smog pollution in China: a case study. J. Clean. Prod. 112, 1627–1634.
Wolter, K., Timlin, M.S., 1998. Measuring the strength of ENSO events: how does 1997/98 rank? Weather 53 (9), 315–324.

Xia, X., Che, H., Zhu, J., Chen, H., Cong, Z., Deng, X., Fan, X., Fu, Y., Goloub, P., Jiang, H., Liu, Q., Mai, B., Wang, P., Wu, Y., Zhang, J., Zhang, R., Zhang, X., 2016. Ground-based remote sensing of aerosol climatology in China: aerosol optical properties, direct radiative effect and its parameterization. Atmos. Environ. 124, 243–251.

Xiao, Q., Zhang, H., Choi, M., Li, S., Kondragunta, S., Kim, J., Holben, B., Levy, R.C., Liu, Y., 2016. Evaluation of VIIRS, GOCI, and MODIS Collection 6 AOD retrievals against ground sunphotometer observations over East Asia. Atmos. Chem. Phys. 16 (3), 1255–1269.

Xiao, Z., Liang, S., Wang, J., Jiang, B., Li, X., 2011. Real-time retrieval of Leaf Area Index from MODIS time series data. Rem. Sens. Environ. 115 (1), 97–106.

Yu, H., Remer, L.A., Chin, M., Bian, H., Kleidman, R.G., Diehl, T., 2008. A satellite-based assessment of transpacific transport of pollution aerosol. J. Geophys. Res.: Atmos. 113, D14S12.

Zhang, J., Reid, J.S., 2010. A decadal regional and global trend analysis of the aerosol optical depth using a data-assimilation grade over-water MODIS and Level 2 MISR aerosol products. Atmos. Chem. Phys. 10 (22), 10949–10963.

Zhang, Z.Y., Wong, M.S., Nichol, J., 2016. Global trends of aerosol optical thickness using the ensemble empirical mode decomposition method. Int. J. Climatol. 36 (13), 4358–4372.

Zhou, G., Liu, S., Li, Z., Zhang, D., Tang, X., Zhou, C., Yan, J., Mo, J., 2006. Old-growth forests can accumulate carbon in soils. Science 314 (5804), 1417-1417.